7-1-2009

Multipoint, high time resolution galactic cosmic ray observations associated with two interplanetary coronal mass ejections

Andrew P. Jordan
A.P.Jordan@unh.edu

Harlan E. Spence
Boston University, harlan.spence@unh.edu

J. B. Blake

T. Mulligan

D. N. A. Shaul

See next page for additional authors

Authors

Andrew P. Jordan, Harlan E. Spence, J. B. Blake, T. Mulligan, D. N. A. Shaul, and M. Galametz

Multipoint, high time resolution galactic cosmic ray observations associated with two interplanetary coronal mass ejections

A. P. Jordan,[1] H. E. Spence,[1] J. B. Blake,[2] T. Mulligan,[2] D. N. A. Shaul,[3] and M. Galametz[4]

[1] Galactic cosmic rays (GCRs) play an important role in our understanding of the interplanetary medium (IPM). The causes of their short timescale variations, however, remain largely unexplored. In this paper, we compare high time resolution, multipoint space-based GCR data to explore structures in the IPM that cause these variations. To ensure that features we see in these data actually relate to conditions in the IPM, we look for correlations between the GCR time series from two instruments onboard the Polar and INTEGRAL (International Gamma Ray Astrophysical Laboratory) satellites, respectively inside and outside Earth's magnetosphere. We analyze the period of 18–24 August 2006 during which two interplanetary coronal mass ejections (ICMEs) passed Earth and produced a Forbush decrease (Fd) in the GCR flux. We find two periods, for a total of 10 h, of clear correlation between small-scale variations in the two GCR time series during these 7 days, thus demonstrating that such variations are observable using space-based instruments. The first period of correlation lasted 6 h and began 2 h before the shock of the first ICME passed the two spacecraft. The second period occurred during the initial decrease of the Fd, an event that did not conform to the typical one- or two-step classification of Fds. We propose that two planar magnetic structures preceding the first ICME played a role in both periods: one structure in driving the first correlation and the other in initiating the Fd.

1. Introduction

[2] Galactic cosmic rays (GCRs) play an integral role in our understanding of the interplanetary medium (IPM). Through a series of balloon experiments, Victor Hess in 1912 first demonstrated that these energetic particles originate from an extraterrestrial source. From his discovery to the start of the space age, GCR measurements remained one of the only ways to directly sample the IPM [*Parker*, 2001]. Because of this, GCRs have been foundational in increasing our knowledge about the IPM.

[3] GCRs are ions and electrons accelerated outside the heliosphere to energies of at least the order of 100 MeV. The GCRs of interest to this study, that is, those having energies on the order of 100 MeV, have speeds much higher than that of the solar wind and scattering mean free paths much less than the size of the heliosphere. Therefore, the flux of these GCRs at 1 AU can be assumed to be isotropic [*Jokipii and Kóta*, 2000]. Even such low-energy GCRs have gyroradii comparable to the characteristic dimension of Earth's magnetosphere under typical IPM conditions (270 Mm or 40 R_E for a 100 MeV proton in a 5 nT field). Thus, for a structure in the IPM to noticeably influence these GCRs, it must have a size scale at least similar to that of the magnetosphere.

[4] Measuring GCRs has greatly benefited our current knowledge of the IPM on all size scales throughout the heliosphere. Prior to the discovery of the solar wind and interplanetary magnetic field (IMF), *Forbush* [1937] observed a geomagnetic storm that was concurrent with a decrease in GCR fluxes measured on the ground at two separate ionization chambers. This phenomenon was later termed a Forbush decrease (Fd) and emphasized the importance and utility of GCR data. Ensuing attempts to understand the cause of Fds revealed that the flux of GCRs is anticorrelated with sunspot number [*Forbush*, 1954]. *Parker* [1958a] described the average structure of the IPM using the discovery by *Biermann* [1951, 1957] of a continuous stream of particles emanating from the Sun. He then accounted for the observed 11-year cycle in GCR flux with a model

---

[1]Department of Astronomy, Boston University, Boston, Massachusetts, USA.
[2]The Aerospace Corporation, El Segundo, California, USA.
[3]High Energy Physics Group, Department of Physics, Imperial College London, London, UK.
[4]Laboratoire AIM, Université Paris Diderot, DAPNIA, Service d'Astrophysique, CEA, DSM, CNRS, Gif-sur-Yvette, France.

wherein GCRs would experience increased diffusion near solar maximum because of increased irregularities in the IMF [*Parker*, 1958b]. This diffusion would tend to scatter the GCRs out of the inner heliosphere and create a minimum in their flux.

[5] Long-term studies revealed that, in addition to the 11-year solar cycle, the 22-year cycle also affects GCRs [*Jokipii and Thomas*, 1981]. During solar minima of positive polarity ($A > 0$), that is, when the IMF is directed out of the Sun's northern hemisphere, the GCR flux reaches a flat-topped maximum. When a solar minimum occurs during periods of negative polarity ($A < 0$), however, the maximum in GCR flux is more peaked. During $A > 0$, GCRs enter the heliosphere by gradient-curvature drifting down over the poles of the Sun and out along the heliospheric current sheet, which divides the two regions of opposite magnetic polarity. They travel in along the current sheet and out above the poles when $A < 0$. Simulations by *Jokipii and Thomas* [1981] showed that the involvement of the current sheet accounts for these alternating maxima in GCR flux, as previously suggested by *Kóta* [1979]. When GCRs enter the heliosphere along the current sheet during $A < 0$, the current sheet plays an important modulating role, thus creating the peaked maximum. During the opposite polarity, however, the GCRs have preferred access above the poles and so are less affected by the sheet in the inner heliosphere. In this case the GCR intensity reaches maximum more quickly. Recent Ulysses observations of GCR latitudinal gradients, however, suggest that this simple picture is incomplete [*Heber et al.*, 2008].

[6] Although Fds furthered understanding of the very large-scale IPM, the events have also been invaluable for learning about the smaller scales. Initially, none knew whether the geomagnetic field itself or an external disturbance decreased the GCR flux during geomagnetic storms. *Simpson* [1954] discovered that GCR modulation does have an external source, and *Morrison* [1956] subsequently suggested that a plasma cloud ejected from the Sun could both shield the Earth from cosmic rays and compress the geomagnetic field. This was observationally shown to be the case once simultaneous in situ and ground-based measurements could be made [*Coleman et al.*, 1960; *Fan et al.*, 1960] and interplanetary coronal mass ejections (ICMEs) were directly detected.

[7] GCRs thus provide a good proxy for determining the passage of an ICME [*Cane*, 2000]. Studies have further differentiated GCR modulation driven by the sheath region from modulation caused by the ejecta of an ICME [*Barnden*, 1973a, 1973b]. Strong shocks can precede a sheath of highly turbulent field that may increase diffusion enough to enhance GCR transport from the region, thereby decreasing the GCR flux. The closed and high magnetic field of the subsequent ejecta provides further shielding that decreases the flux even more. GCR measurements can then categorize ICMEs into two groups: those causing one-step Fds and those causing two-step Fds. The passage of an ICME with a weak or with no shock or the passage of a shock but no ejecta may cause a one-step Fd. If both the shock and the ejecta pass Earth, a two-step Fd may be seen.

[8] Some have attempted using GCRs to study the internal structure of the ICMEs themselves. These analyses utilize multiple ground-based neutron monitors to analyze anisotropies in GCR fluxes during the passage of the ejecta. Although difficult, such work may provide helpful information about field orientations and connectivity [*Cane*, 2000, and references therein; *Munakata et al.*, 2003; *Kuwabara et al.*, 2004].

[9] Other analyses have focused on not only the small-scale structure of ICMEs but also the small-scale features in the magnetic field of the IPM. They have concluded that scintillation, on timescales of minutes to hours, in GCR fluxes is the result of IMF turbulence [*Dhanju and Sarabhai*, 1967; *Jokipii*, 1969; *Owens and Jokipii*, 1972, 1973; *Nagashima et al.*, 1990; *de Koning*, 2003; *de Koning and Bieber*, 2004; *Starodubtsev and Usoskin*, 2003; *Starodubtsev et al.*, 2005, 2006; *Grigoryev et al.*, 2008]. Deriving more specific information from GCR data about the three-dimensional IMF, though, has proved a challenging task [*de Koning and Bieber*, 2004].

[10] Most of the above work focuses on GCR modulation timescales that last longer than a day, corresponding to size scales greater than 50,000 Mm (0.3 AU or 8000 R_E). Analyses of solar cycle variations or of the overall structure of Fds are examples of such work. Fewer attempts have been made to understand shorter variations on the order of an hour or less (size scales of about a few thousand megameters). Such studies, like those of GCR scintillation, tend to concentrate mainly on the spectra of the variations. Very little work, other than analyses of GCR anisotropies during ICMEs, has focused on short and small scales in the time domain by attempting to discover one-to-one correspondence between short-scale GCR variations and small-scale features in the IPM. Furthermore, since the anisotropy studies mentioned above use hourly averaged data, they may miss many such small-scale correlations.

[11] In this paper, we probe this important but largely unexplored area by comparing high time resolution space-based GCR and IPM data. This is a necessary next step in the attempt to understand GCR modulation [*Storini*, 2000]. After identifying periods of small-scale GCR variations that are clearly due to inferred IPM structures, we examine the IPM time series for correlations with the GCR data, searching especially for relations that have thus far remained undiscovered and unexplained.

2. Two-Point, Space-Based GCR Measurements
2.1. Polar and INTEGRAL Satellites

[12] We use space-based instruments rather than ground-based neutron monitors because the former are better suited to detect GCR variations on the timescales of interest. Historically, ground-based neutron monitors have been some of the primary instruments for collecting GCR data. They are not, however, ideal for small-scale studies. First, due to magnetospheric and atmospheric shielding [*Shea and Smart*, 1990], most neutron monitors are sensitive only to GCRs with energies greater than ~500 MeV. The IPM structures in which we are interested are too small to modulate GCRs with these energies and are thus undetectable with neutron monitors. Second, the magnetosphere has a complex effect on GCRs. The magnetosphere could play an important role, not just in rerouting GCR [*Smart et al.*, 2000], but also in modulating them on short timescales. Using only neutron monitors without concurrent measurements
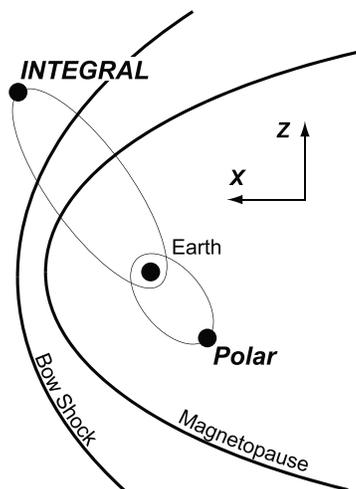
Figure 1. Polar and INTEGRAL orbit in roughly the same *xz* plane. Polar stays within the magnetosphere, while INTEGRAL is generally outside. At apogee, Polar is located at about $-6\ R_E\ \hat{x}$ and $-7\ R_E\ \hat{z}$, and INTEGRAL is located at about $14\ R_E\ \hat{x}$ and $19\ R_E\ \hat{z}$ in Geocentric-Solar-Ecliptic coordinates, as shown.

outside the magnetosphere makes such an effect, if it exists, difficult or even impossible to detect. Finally, most neutron monitors experience a significant diurnal effect that can make resolving small-scale variations difficult.

[13] Instruments onboard spacecraft, on the other hand, do not have the same limitations. The small mass of the spacecraft does not provide sufficient shielding against even low-energy GCRs. Thus, spaceborne instruments can typically detect GCRs with energies an order of magnitude less than 1 GeV and therefore have the potential to resolve small-scale IPM structures [*McDonald*, 2000]. Structures large enough to affect GCRs at such energies can pass Earth in a few minutes. The atmospheric cutoff isclearly irrelevant to such instruments. The magnetosphere should also be unimportant in affecting the observations if the spacecraft orbit is beyond the geomagnetic cutoff for GCR energies of interest. Although employing GCR data from spacecraft to study the IPM is not new [*McDonald*, 2000, and references therein], such analyses typically use hourly or longer averages and look at large scales (ICMEs and larger). The Ulysses mission, the two Voyager spacecraft, some of the Pioneer spacecraft, IMP-8, and the GOES spacecraft all have instruments designed to detect particles with GCR energies. They do not, however, have the geometric factors required for a high signal-to-noise ratio at time resolutions less than an hour. Those using their data have not attempted to quantify or search for the causes of shorter-scale GCR variations.

[14] To ensure that features we see in the space-based GCR time series actually relate to conditions in the IPM, we use GCR data from two instruments onboard the Polar and INTEGRAL (International Gamma Ray Astrophysical Laboratory) satellites, respectively inside and outside Earth's magnetosphere (see Figure 1). Though Polar is always inside the magnetosphere, it is generally at positions beyond the geomagnetic cutoff of interest here, thus minimizing any magnetospheric effects. In the events we study, both space-

craft are typically located at about the same Geocentric-Solar-Ecliptic (GSE) $\hat{y}$ location, with INTEGRAL having a larger $\hat{x}$ and $\hat{z}$ position ($\hat{x}$ is along the Sun-Earth line, and $\hat{z}$ is the ecliptic North Pole).

[15] For correlations to exist between the time series of the spacecraft, three conditions need to be fulfilled. First, if we were to ignore the magnetosphere, the IPM conditions must be identical at both spacecraft. In the case of Polar and INTEGRAL, the separation between them lies mostly along $\hat{x}$ and $\hat{z}$, so the IPM needs to be unchanging over those distances. Furthermore, such an IPM structure must extend far enough beyond both spacecraft (at least two gyroradii in any direction perpendicular to the IMF) that a neighboring structure cannot modulate any detected GCRs at one of the spacecraft and not at the other. Second, as previously mentioned, the magnetosphere cannot play an important role in affecting the GCR flux as detected by Polar. Otherwise, the variations seen at Polar would be the result of both the IPM and the magnetosphere, thus breaking down the correlation between the two spacecraft. Finally, the modulated GCRs must fall within the energy range detectable by both instruments. If the environments in both the IPM and the magnetosphere meet all three requirements, then we expect to observe a correlation. The more likely case, however, is that at least one condition will be unmet at a given time, thereby keeping such correlations from being a common and easily discernable occurrence.

2.2. Instruments

[16] We describe the Polar and INTEGRAL spacecraft and instrumentation only insofar as they are used to measure the time history of the intensity of the GCRs. Polar and INTEGRAL did not have GCR studies as an objective. Therefore, we employ these two missions as sensors of opportunity, using as our signal what for their prime mission objectives are background events.

[17] The NASA Polar spacecraft launched on 24 February 1996 into an orbit with an inclination of 86 degrees, an apogee of 9 R_E, and a perigee of 1.8 R_E geocentric. Its entire orbit is thus within the magnetosphere. Initially apogee was at high northern latitudes, but it then slowly precessed (∼16 degrees/year) to the equator and then to high southern latitudes. In this paper we discuss measurements made in the summer of 2006 when the satellite apogee was over the southern polar cap (see Figure 1).

[18] One of the twelve investigations aboard Polar is CEPPAD (Comprehensive Energetic Particle Pitch Angle Distribution), which contains three detector systems [*Blake et al.*, 1995]. The one of interest for GCR studies is the High Sensitivity Telescope, or HIST [*Contos*, 1997]. The primary purpose of HIST is measuring energy spectra and angular distributions of energetic radiation belt electrons in the energy range from ∼1 to 10 MeV. A secondary objective is analyzing the proton population from ∼5 to 100 MeV.

[19] To make these observations, HIST comprises three detectors. The first two are silicon surface-barrier detectors with thicknesses of 324 micrometers and 2000 micrometers, respectively. The third detector is a plastic scintillator with a photomultiplier tube viewing it from behind. The goal of containing the energy deposit of up to 10 MeV electrons determined the shape and volume of the scintillator.
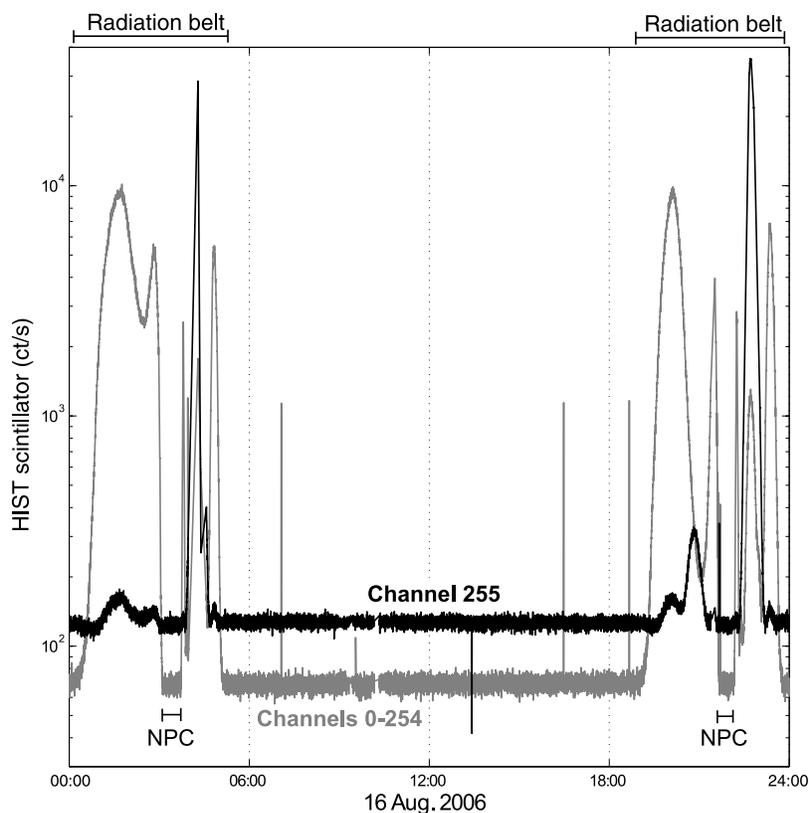
Figure 2. The count rate of the Polar/HIST scintillator for the day 16 August 2006. The sum of the rates in the lowest-energy channels, 0–254, is plotted in gray. The overflow channel, Channel 255, is plotted in black. The two radiation belt passages and the low-altitude passages over the northern polar cap ("NPC") are labeled. When not in the radiation belts, the scintillator cleanly measures GCRs in Channel 255.

[20]   In this paper we do not use HIST in its primary mode as a particle telescope. Rather, we analyze only the count rate in the plastic scintillator; that is, we utilize the scintillator as an omnidirectional sensor. The scintillator has a geometric factor of 465 cm^2 sr [*Contos*, 1997]. HIST digitizes the amplitude of each event in the scintillator into 256 channels (0 to 255) from ∼100 keV to 10 MeV. All pulses larger than 10 MeV go into Channel 255, the overflow channel. The plastic scintillator is sufficiently large such that most GCRs deposit well over 10 MeV. Therefore primary GCR events appear mainly in Channel 255 with the exceptions of "corner cutters" and particles that just reach the scintillator after depositing most of their energy elsewhere in the spacecraft.

[21]   Figure 2 is a plot of the HIST scintillator data for 16 August 2006. The time history is typical, and we show this specific day only because the radiation belt passages occurred at the beginning and end of the day. The radiation belt passages differ significantly in detail from one another, but the presence of magnetospheric particles is readily seen. For an approximately 14 h period, from ∼0500 to 1900 UT, Polar was at high southern latitudes, and the scintillator was able to observe GCRs without the radiation belt background. As expected, during this interval the majority of events (∼60%) had energy deposits >10 MeV and appeared in Channel 255. In the middle of the radiation belt passages, Polar was at low altitude on open field lines in the north (labeled "NPC" for the northern polar cap). HIST cleanly detects GCRs during these times as well.

[22]   In summary, the orbit of Polar is such that it spends approximately two-thirds of its orbital period outside the radiation belts where the only energetic particles to be found are GCRs, excluding solar energetic particles. Therefore, the only response of HIST during these times is a background count rate caused by the GCRs. HIST usually counts over one hundred background events each second, creating a ten percent statistical uncertainty in the highest time resolution observations available (1.5 s).

[23]   The other instrument we use is the Spectrometer on INTEGRAL (SPI). INTEGRAL is an ESA gamma ray observatory that launched on 17 October 2002. Its 3-day orbit has an apogee of ∼24 R_E, a perigee of ∼1.4 R_E, and an inclination of 51.6 degrees (see Figure 1). The purpose of the high apogee is to minimize the time INTEGRAL spends in the Earth's radiation belts; thus, the spacecraft is outside the magnetosphere for much of its orbit.

[24]   SPI consists of an array of 19 actively cooled germanium detectors. Each Ge detector is hexagonal in shape and has a side length of 3.2 cm and height of 7 cm [*Vedrenne et al.*, 2003]. An anticoincidence shield (ACS) made of 91 bismuth germanate oxide blocks surrounds the Ge detectors. Cosmic rays can interact directly with the Ge detectors or with materials on the spacecraft. Their interactions produce a background that varies due to modulations of the incident GCR flux. The magnitude of this variation is typically of the same order as that of the 511 keV gamma ray signal from the Galactic center, which is a primary INTEGRAL observation goal [*Teegarden et al.*,
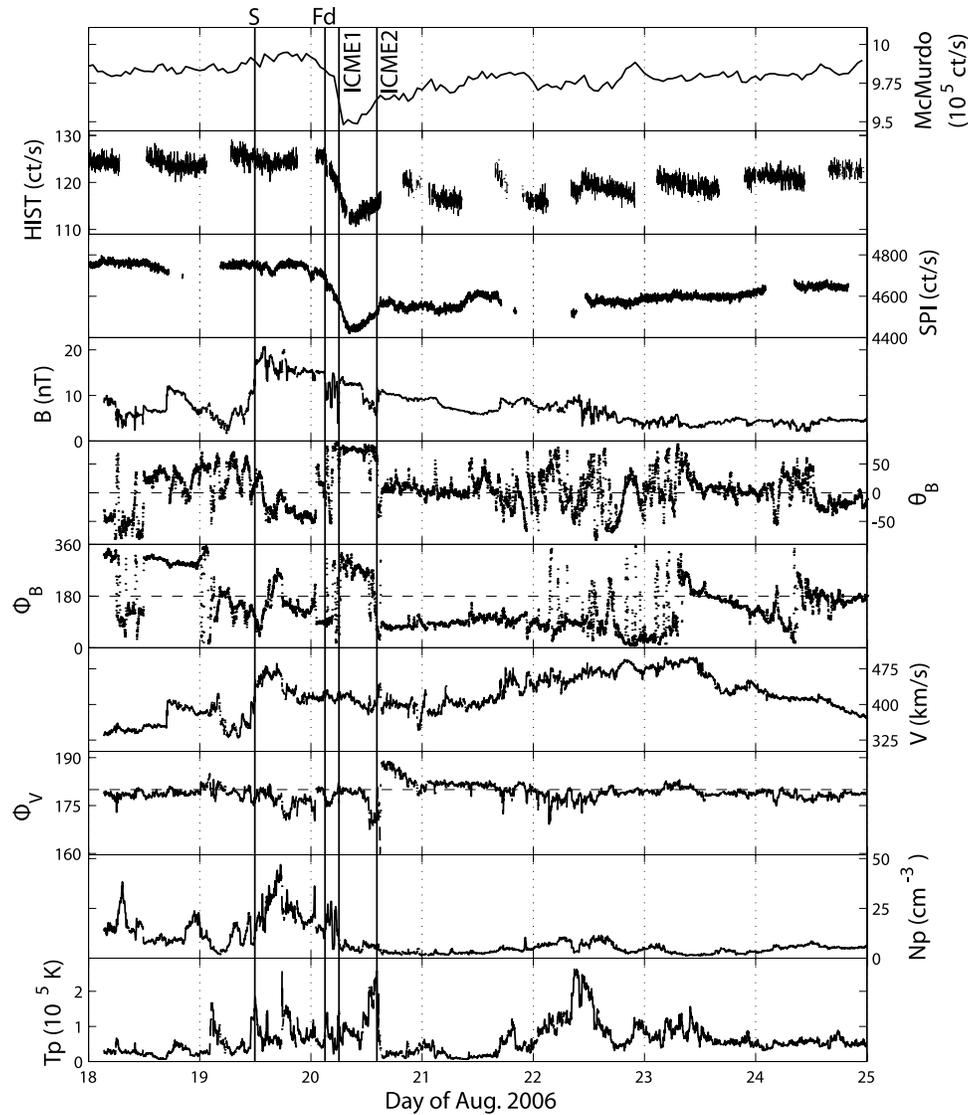
Figure 3. The first, second, and third panels show the GCR data, while the others show the ballistically propagated IPM data from ACE (all times are UT). The first panel is a plot of GCR data from the neutron monitor at McMurdo Station in Antarctica. The second and third panels show 1 min GCR count rates from HIST and SPI, which have uncertainties too small to show here, about ±1 ct/s and ±9 ct/s, respectively. The data gaps in both occur when each spacecraft passes through the radiation belts. θ_B is the IMF vector's latitude with respect to the ecliptic plane, and ϕ_B is its angle in the ecliptic plane with respect to GSE $\hat{x}$ (180° is antisunward). ϕ_V is the angle in the ecliptic plane of the solar wind direction. Np is the proton number density, and Tp is the radial proton temperature. The shock, start of the Fd, first ICME, and second ICME are labeled as "S," "Fd," "ICME1," and "ICME2," respectively.

2004]. INTEGRAL experimenters must use these same background signals to ensure that GCR variations are reliably subtracted from the gamma ray signal [*Teegarden et al.*, 2004; *Jean et al.*, 2003]. Consequently, the SPI detectors are excellent monitors of GCRs, and we use them in the present work to analyze short-term variability in the GCR flux.

[25] The SPI signals available for GCR detection are the amplitude saturations of the detector systems. These include the saturated count rates in the ACS (ACSSAT) and the Ge detectors (GEDSAT). While the count rates of both are available, for this paper we use only the GEDSAT rates. The Ge detectors saturate at ~10 MeV, resulting in effective

GEDSAT cosmic ray energy threshold of ~200 MeV. This is a consequence of the energy required to penetrate the spacecraft shielding and still reach the Ge detectors with enough remaining energy to deposit at least 10 MeV [*Teegarden et al.*, 2004]. The GEDSAT data have a time resolution of 1 s. The large geometric factor of SPI provides an average GCR count rate about forty times greater than that of the HIST scintillator. As with HIST, particles in the radiation belts overwhelm the GCR signal, so we remove periods when INTEGRAL is passing through the belts. SPI is also sensitive to solar energetic particle events, which we avoid in this study.
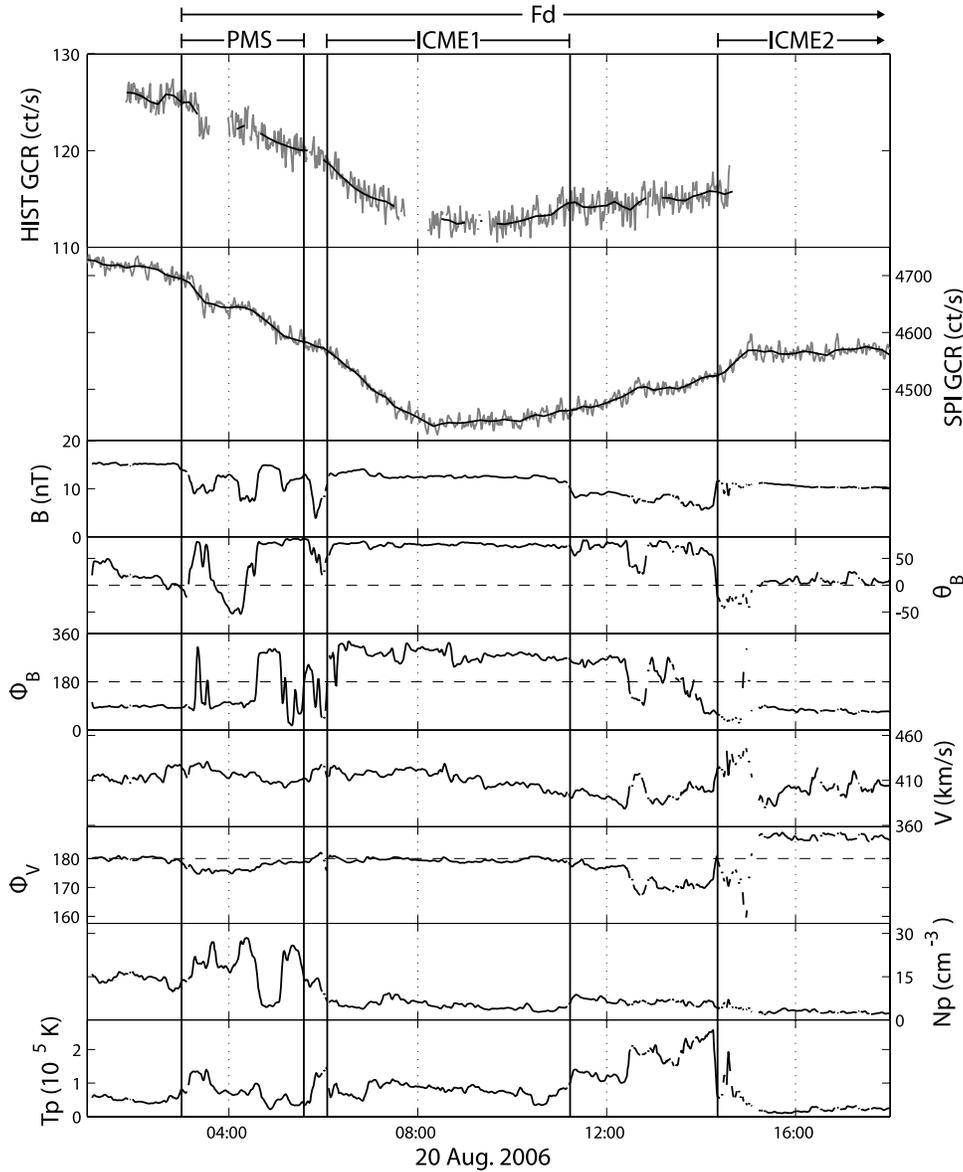
Figure 4. The first and second panels show the beginning and minimum of the Fd as seen in the GCR data (1 min data in gray and 10 min resampling in black). The 1 and 10 min HIST data have respective uncertainties of about ±1 and ±0.5 ct/s. The same for SPI are about ±9 and ±3 ct/s. The minimum was associated with the arrival of ICME1. The arrival of ICME2 near 1500 UT accompanied a simultaneous interruption of the recovery of the GCR count rate from the Fd, as shown in the SPI data. The region of planar magnetic structure is labeled "PMS."

[26] All solar wind and IMF data come from the Advanced Composition Explorer (ACE). For this study, we ballistically propagate the IPM parameters to the magnetosphere using only the $\hat{x}$ component of the solar wind velocity and assuming its constancy between the location of ACE and the magnetosphere. This simple method of propagation is sufficient for this study, as the timing inaccuracies so introduced are much shorter than the timescales of the GCR variations we find.

3. Observations and Analysis

[27] We analyze the period of 18–24 August 2006 (shown in Figure 3), during which two ICMEs passed

Earth. They occurred during a quiet period near solar minimum. SOHO/LASCO observed two halo CMEs separated by 9 h on 16 August. Their ICME counterparts did not have associated SEP events, so the GCR signal had no interference from such high-energy particles. The shock of the first ICME (ICME1) arrived at about 1200 UT on 19 August (line "S" in Figure 3). The sheath region lasted for over half a day, ending with the arrival of the ejecta around 0600 UT on 20 August. A rotation in the IMF, followed by a region of enhanced and low variance field, marked the arrival of ICME1. It lasted about 5 h and was followed by the second ICME (ICME2), which began at about 1400 UT. A sharp IMF rotation, decrease in the proton temperature, and flow deflection all signaled its
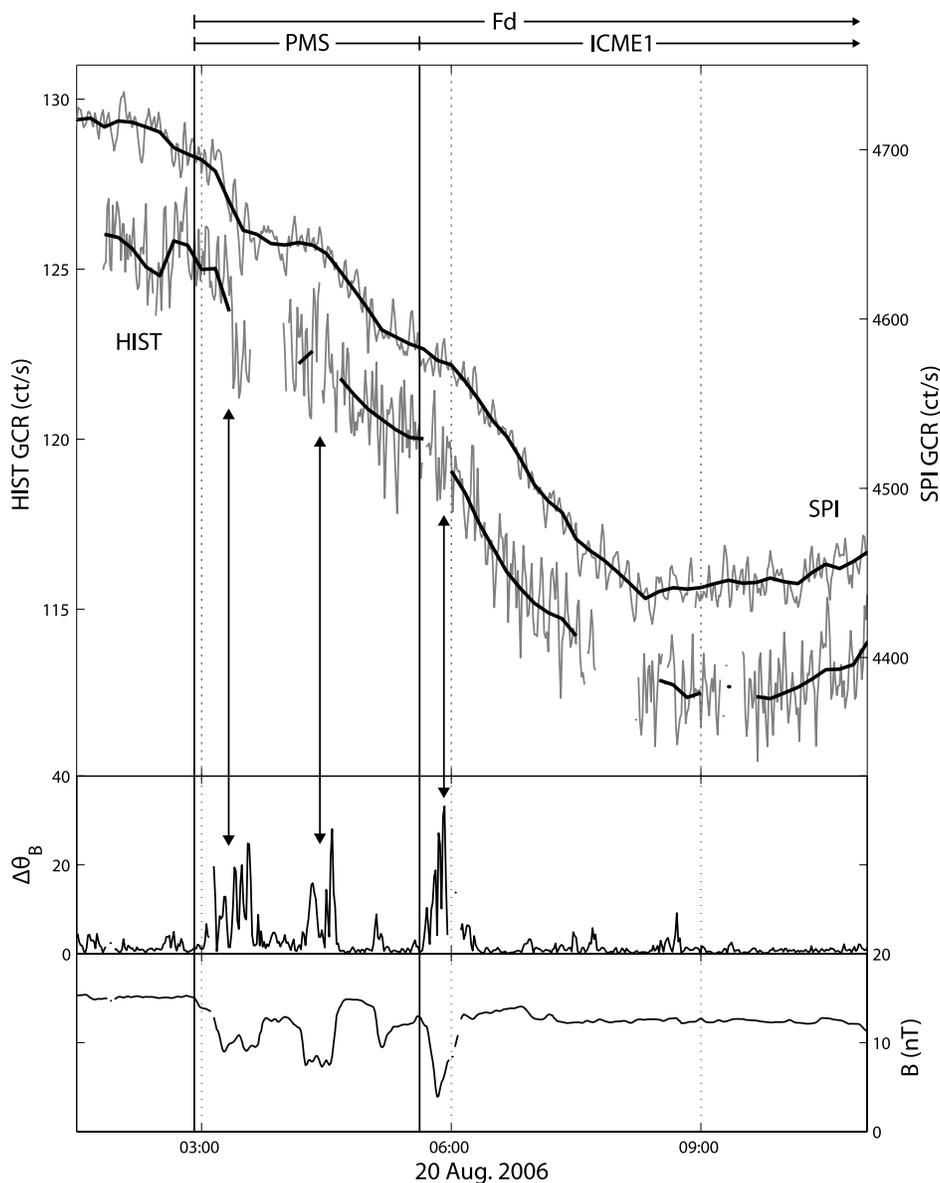
Figure 5. (top) The GCR data from SPI and HIST (1 min data in gray and 10 min resampling in black). The 1 and 10 min HIST data have respective uncertainties of about ±1 and ±0.5 ct/s. The same for SPI are about ±9 and ±3 ct/s. Three steps can be seen in both data sets. $\Delta\theta_B$ is the total angular change between consecutively measured IMF vectors. (bottom) The three peaks in $\Delta\theta_B$ accompanied by minima in the field strength between 0300 and 0600 UT indicate regions of large field rotations. The first two series of rotations are part of the planar magnetic structure, labeled "PMS," and the third is concurrent with the arrival of ICME1.

arrival; *Wimmer-Schweingruber et al.* [2006] summarize how these characteristics relate to ICMEs. ICME2 lasted for about a day. Throughout both events, the solar wind speed remained nearly constant. It peaked at a speed of 470 km/s at the shock but then leveled off to about 400 km/s.

[28] The events produced an approximately week-long Fd evident in both ground- and space-based GCR data. A comparison of the two time series from HIST and SPI to that from the neutron monitor at McMurdo Station (first, second, and third panels of Figure 3) confirms that the satellite instruments do indeed detect GCRs, although at lower energies. The decrease beginning near 0300 UT of

20 August and the interruption of the recovery at 1500 UT of the same day are the most obvious features common to the three data sets.

[29] A word must be said about defining the time of the Fd initiation. Because the neutron monitor data have 1-h resolution, they are insufficient to identify the start of the Fd to within less than a couple hours. HIST and SPI are thus more reliable for defining the start time. Although a gap occurred in the HIST data at the beginning of 20 August, the time series still had 2 h of continuous data before the decrease at 0300 UT (marked by the line labeled "Fd"). The average count rate during those 2 h was about the same as
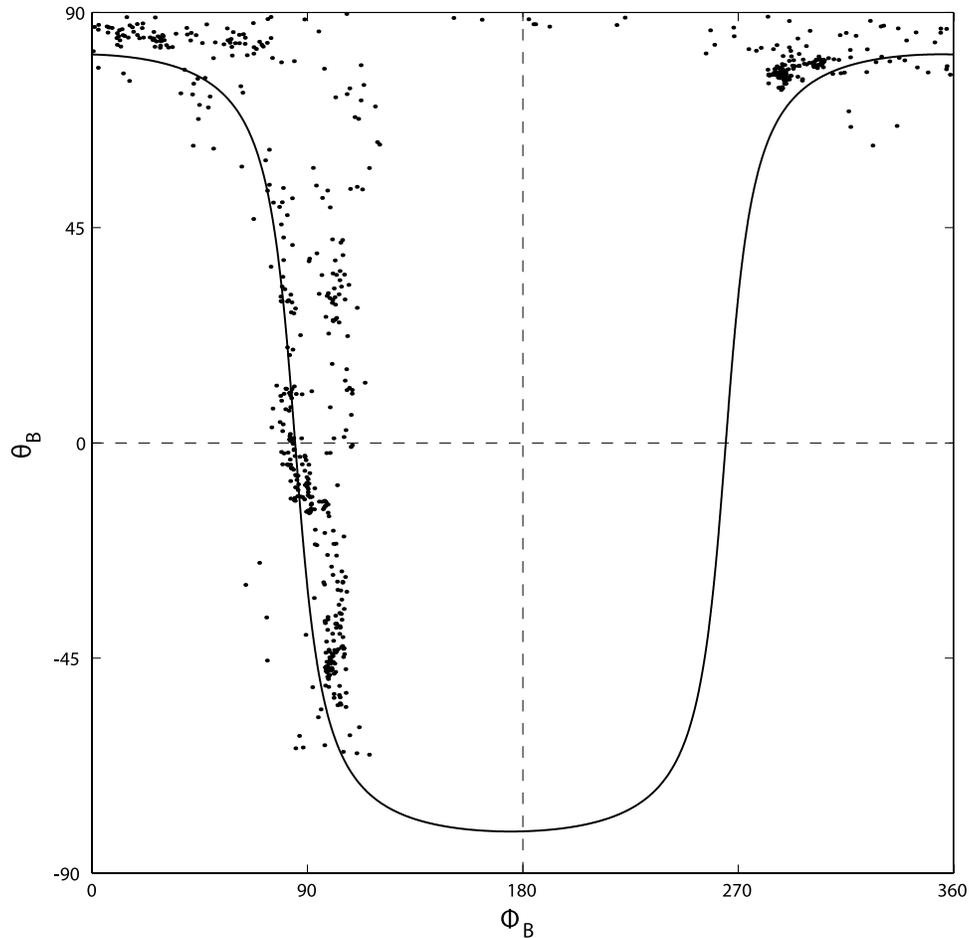
Figure 6. The points on this scatterplot show the angular coordinates of the magnetic field direction measured by ACE (16 s data) from about 0300 to 0530 UT on 20 August. They lie along the curve given by $n_x \cos\theta \cos\phi + n_y \cos\theta \sin\phi + n_z \sin\theta = 0$ [*Neugebauer et al.*, 1993], where the vector (n_x, n_y, n_z) is the direction of minimum variance and is normal to the plane in which the IMF vectors lie. In this case the vector was $(-1, 0, 0)$ in GSE coordinates.

that of the data preceding the gap, which suggests that the Fd began at 0300 UT. In SPI, the GCR flux began to decrease slowly after 0000 UT. Since a similar gradual decrease did not occur in the HIST data, it appeared to be a GCR modulation local to SPI. The time series began to correlate with that from HIST only at the sharper drop at 0300 UT. Therefore, we define that time to mark the start of the Fd.

[30] The event, however, did not fall into either Fd category of one- or two-step decreases. Neither the shock nor ICME1 initiated the first decrease in the GCR count rates, which reached a minimum at 0800 UT on 20 August. The shock passed Earth half a day before the Fd began. ICME1, evidenced by a strong magnetic field with low variance, did not arrive until about halfway through the initial decrease of the Fd. Because the decrease began when the spacecraft was more than 100 GCR gyroradii from the shock and more than 10 gyroradii from ICME1, the cause of the Fd is, at this point, unclear. The interruption of the GCR recovery at 1500 UT was associated with the ICME2. It occurred well after the count rates had already reached a minimum. To better understand this unusual and structured event, we now focus on smaller scales.

[31] Though we are searching for GCR correlations on these small scales, it is important to note that such correlations were not common during the time analyzed. As explained above, this is anticipated. We find only two periods, a total of 10 h, of clear correlation between HIST and SPI during these 7 days.

[32] One period of correlation occurred on 20 August during the beginning of the Fd (see Figure 4). As mentioned above, this Fd did not fit into either category of one- or two-step Fds since neither the shock nor the ejecta drove the initial decrease in GCR count rates. The Fd began near 0300 UT in both HIST and SPI, about 15 h after the shock and 3 h before ICME1. Furthermore, the Fd, as seen in the HIST and SPI data, actually consisted of three steps that were too close together to be seen in 1 h resolution data. Figure 5 shows these steps, which are labeled with arrows.

[33] The last of these steps was associated with the passage of the ICME itself. A rapid rotation of the magnetic field direction, seen as an increase in $\Delta\theta_B$ and marked by the third arrow, occurred prior to 0600 UT; it signaled the leading edge of ICME1. As can be seen in the GCR data, the decreasing GCR count rate steepened following this rotation. In both HIST and SPI, the Fd reached minimum
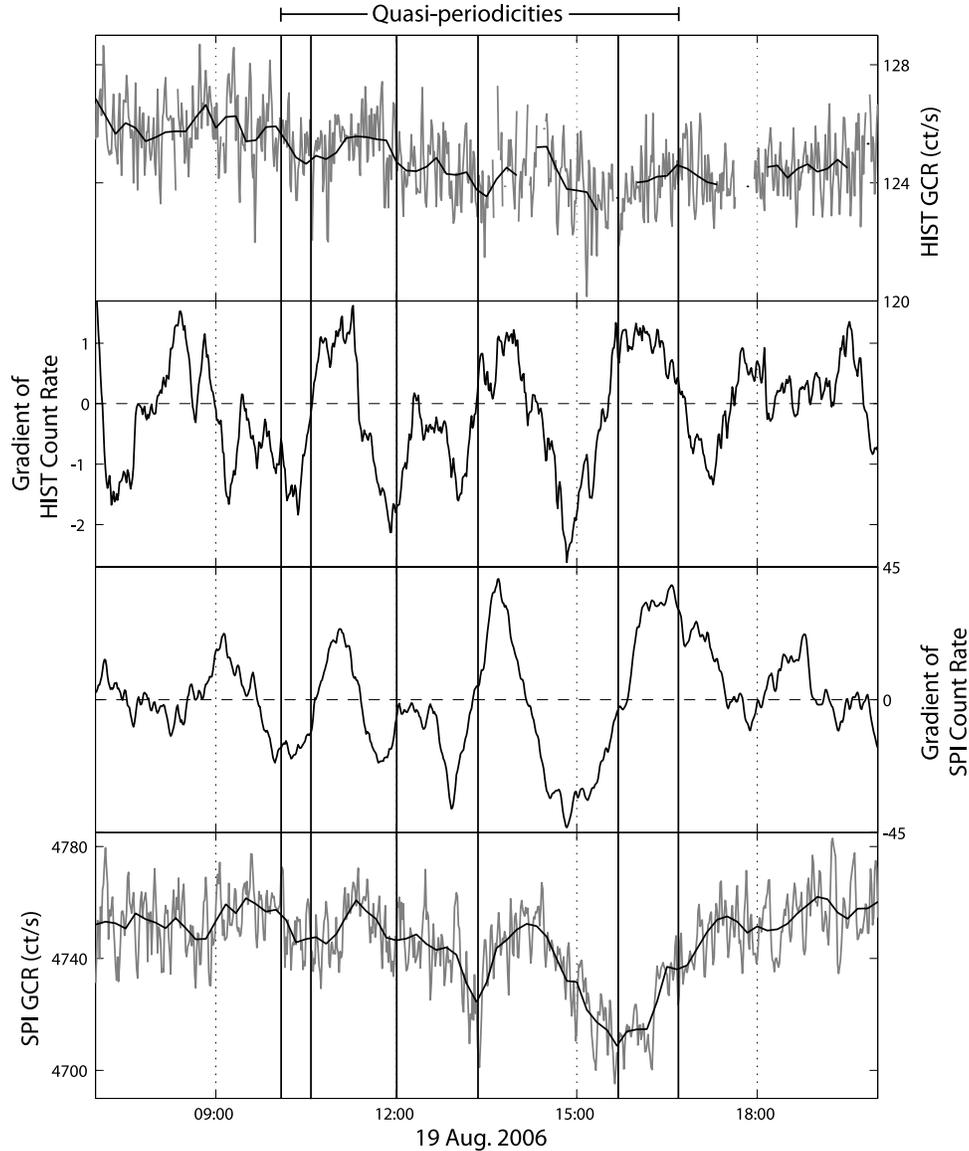
Figure 7. The first and fourth panels show 1 min GCR data (gray) from HIST and SPI overplotted by their 10 min resampling (black). The 1 and 10 min HIST data have respective uncertainties of about ±1 and ±0.5 ct/s. Those for SPI are about ±9 and ±3 ct/s. The second and third panels show the gradients of the GCR data; they have uncertainties of ±0.5 and ±4 ct/s/h, respectively. The gradient is the slope of a linear fit to a 60 min window of data and has units of counts per second per hour. The window was moved one data point for each gradient calculation. The two data sets were well correlated from about 1000 to 1600 UT.

between 0800 and 0900 UT, well within the ICME. This part of the Fd is expected in the classic model: the ejecta provided shielding that decreased the GCR flux [*Cane*, 2000].

[34] The initiation of the Fd, however, did not fit the classic model, since it was unassociated with either the shock of the ICME or the ICME itself. We analyzed the character of the IMF during this period to discover what may have initiated the decrease. This characterization included a minimum variance analysis of the magnetic field data. We utilized the technique described by *Sonnerup and Scheible* [2000]. The direction of minimum variance was nearly aligned with GSE $\hat{x}$ from 0300 to 0530 UT (the region labeled "PMS" in Figure 5), the same time period

that included the first two steps of the Fd. The mid to minimum eigenvalue ratio was roughly six, giving us confidence that the field stayed planar during this period. Thus, though the field direction was changing, as seen in $\Delta\theta_B$, it always remained in the same well defined plane (see Figure 6). For the few hours immediately prior to this period, the IMF was not planar. The planar period ended when ICME1 arrived and therefore coincided with the initiation of the Fd.

[35] *Nakagawa et al.* [1989] first identified similar regions during which the IMF vector remained in the same plane even while significantly rotating. They termed such features planar magnetic structures (PMSs). *Neugebauer et al.* [1993] later did a systematic study of 33 PMSs and found that they
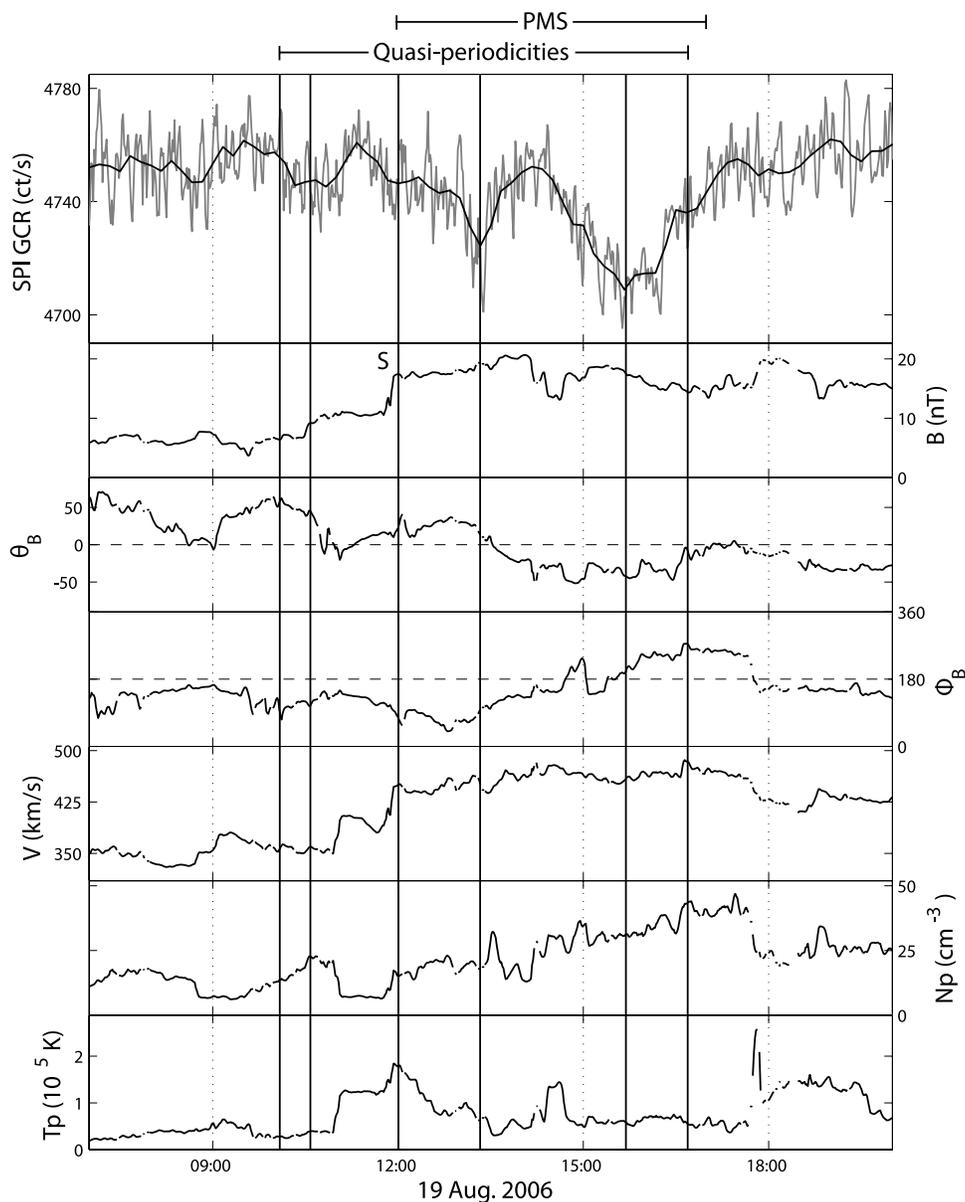
Figure 8. The GCR data from SPI (1 min data in gray and 10 min resampling in black) and the IPM data from ACE are shown. The 1 and 10 min SPI have uncertainties of about ±9 and ±3 ct/s, respectively. The shock of the ICME arrived at noon (labeled as "S" in the second panel showing B).

are compressed or draped features about a disturbance in the IPM. They often occur between an ICME and its shock, as was the case in the 20 August event.

[36] Furthermore, rather than a smooth decrease to the Fd minimum, the GCR data reveal smaller modulations. After the initial decrease at 0300 UT, the SPI count rate remained constant for almost an hour (between the first and second arrows in Figure 5). The HIST data also showed a similar modulation; the data gap, however, may have hidden further variations. Both count rates started decreasing again at about 0430 UT (second arrow). Their slope then began to level out until the arrival of the step associated with the ICME1. At this point the count rates began decreasing more rapidly.

[37] The onset of these first two steps coincided with two intervals of rapid magnetic field rotations. While the timing

is not perfect, we must keep in mind that because of the large gyroradii of GCRs, their local count rate depends on the integrated effects of the nonlocal IMF through which they pass. The local magnetic measurements of ACE are only an estimate of the larger-scale IMF environment modulating the detected GCRs. We therefore do not expect the local, point measurements of the IMF and GCR variations to coincide exactly, even when the two are causally linked. The concurrence suggests that the planar structures shielded the upstream regions from the ambient, or downstream, GCR flux. This is consistent with the conclusions of *Intriligator et al.* [2001, 2008] that PMSs can reduce cross-magnetic-field transport of energetic particles. Whereas previous GCR studies linked the initiation of Fds to the shock and the resulting turbulence or to the ICME itself, neither phenomenon was the evident cause in this case.
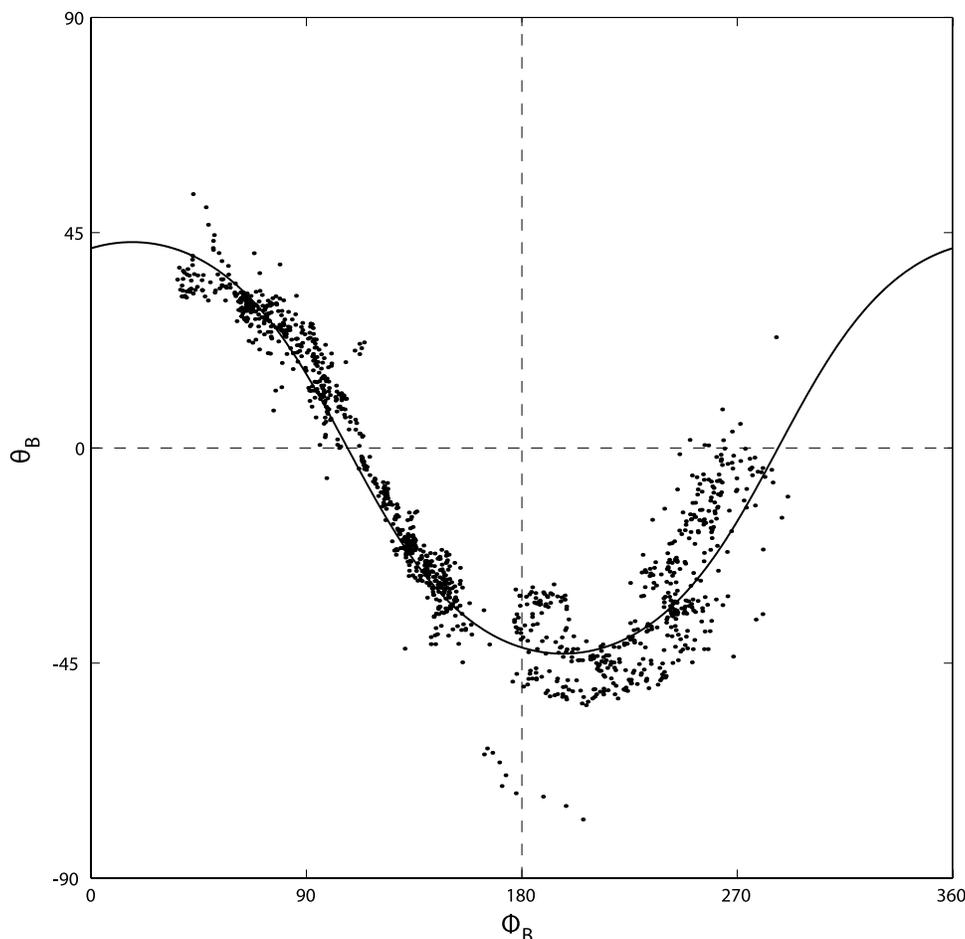
Figure 9. The points on this scatterplot show the angular coordinates of the magnetic field direction measured by ACE (16 s data) from about 1200 to 1700 UT on 19 August. They lie along the curve given by $n_x \cos\theta \cos\phi + n_y \cos\theta \sin\phi + n_z \sin\theta = 0$ [*Neugebauer et al.*, 1993], where the vector (n_x, n_y, n_z) is the direction of minimum variance and is normal to the plane in which the IMF vectors lie. In this case the vector was $(0.7, 0.2, -0.7)$ in GSE coordinates.

While ICME1 did contribute to the final continuation of the decrease, the onset of the Fd began with the planar field rotations. This, together with the concurrent steps and field rotations, implies that the PMS may have initiated the GCR decrease.

[38] The other correlated period began on 19 August near 1000 UT, a day earlier than the Fd, and lasted about 6 h. Figure 7 shows the interval with a few hours plotted on either side. During this time, GCR modulation at both spacecraft went through about four quasi-periodic cycles. The correlation of these cycles is more apparent in the gradients of the two time series, as shown in the second and third panels of Figure 7. Though the two time series are well correlated, they are not identical. This is not surprising for the reasons mentioned in section 2.1.

[39] The reason for the initiation and cessation of this interval is unclear. Nothing in the IMF appeared to initiate the correlation (labeled by the first vertical line in Figure 8). The shock of ICME1 did not pass Polar and INTEGRAL until about 1200 UT, 2 h after the correlation began. The lack of an apparent driver to start this correlation is not surprising. GCRs, because of their large gyroradii (on the order of 100 Mm in this case), respond not to purely local

conditions but to the integrated effect of the regions through which they have passed. Thus, the variations seen with HIST and SPI may not have been directly related to the IMF conditions observed with ACE. Despite this difficulty, some progress in understanding the rest of the event can be made.

[40] The first full quasi-periodic cycle, bounded by the second and third vertical lines, may have been related to a feature seen in the plasma data. The cycle was concurrent with a region immediately preceding the shock. The interval was characterized by constant magnetic field, increased solar wind speed, depressed proton number density, and increased proton temperature. The proton number density decreased by a factor of three, while the proton temperature increased by a factor of three, both with respect to the downstream region. Thus, this interval was in thermal pressure balance with the region preceding it. Why the GCR count rate should have changed in this region is, however, unclear.

[41] As mentioned above, part of the analysis includes searching for PMS. We find a PMS region (labeled in Figure 8) beginning with the shock and ending less than an hour after the period of GCR correlation ended. The mid to minimum eigenvalue ratio was 20, so the IMF was more
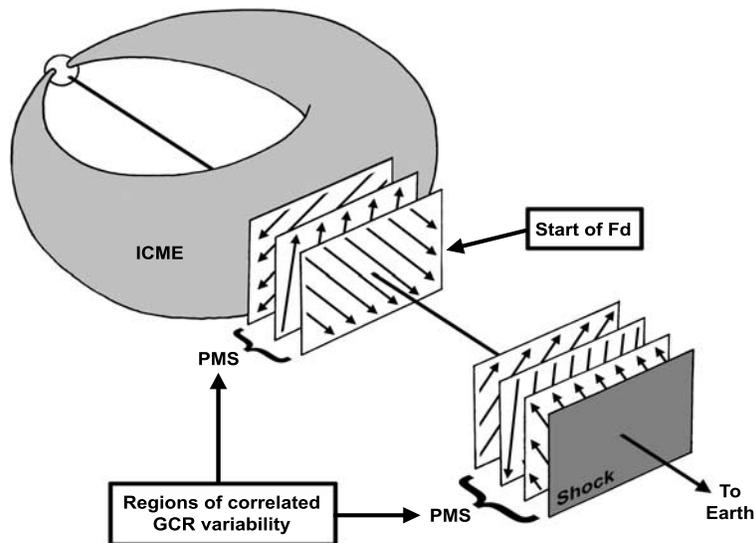
Figure 10. This cartoon, adapted from *Jones et al.* [2002], depicts the first ICME expanding from the Sun (not to scale). It is driving two magnetically planar regions: one immediately following the shock of the ICME and the other immediately preceding the ICME. For clarity, we have not drawn the first PMS with the correct orientation (see Figure 9). Both PMSs were coincident with the intervals of correlated GCR variability, although the first interval did begin 2 h before the shock arrived. The Fd began with the arrival of the second PMS.

planar than the later PMS during the Fd initiation (see Figure 9). The normal of the plane was 0.7 $\hat{x}$, 0.2 $\hat{y}$, and −0.7 $\hat{z}$ at ACE. It is also important to note that no subsequent PMS regions were found until that associated with the initiation of the Fd. Mulligan et al. (2009) link the variations in the GCRs to the shock and subsequent discontinuities and emphasize the importance of magnetic topology to this event. Our discovery that these discontinuities are part of a PMS further confirms that conclusion. As with the initiation of the Fd, a PMS and its substructure appeared to have played an important role in modulating the GCRs.

4. Conclusion

[42] We have analyzed two ICMEs and their ambient IPM and found that a number of features in the two data sets from HIST and SPI were highly correlated both near the shock of the first ICME and during the beginning of the Fd. Since both instruments observed these GCR variations, we have confidence that the modulating structures were indeed in the IPM and were unrelated to magnetospheric effects.

[43] The first period of correlation to occur lasted 6 h and began about 2 h before the shock passed the spacecraft (see Figure 10). It contained approximately four quasi-periodic cycles. We found no compelling relation between the IPM downstream of the shock and the initiation of the correlated interval. We did, however, discover that a PMS following directly after the shock coincided with the rest of the period of correlated GCR variability.

[44] The second period occurred during the initial decrease of the Fd (see Figure 10). Because the initiation of the Fd was unrelated to the passage of either the shock or

the ICME itself, it did not conform to the usual one- or two-step classification of Fds. Instead, the initial decrease was divided into three smaller steps. The last step was associated with the arrival of the first ICME. The first two, however, were concurrent with the passage of a second PMS in the sheath of the ICME. The PMS, which had a normal parallel to the −$\hat{x}$ direction, included two regions of rapid magnetic field rotations. Both of these regions appeared to shield the upstream regions from the downstream GCR flux and create the first two steps in the Fd.

[45] We have thus demonstrated that correlated short-timescale GCR variations are observable using space-based instruments. These variations were present on such short timescales that they would have been difficult to detect with the hourly averaged data used in most studies, emphasizing the importance of using higher time resolution, space-based data. We have also shown that the typical one- and two-step classification and explanation of Fds may not fully encompass the variety of these phenomena, as the scheme ignores the impact of small-scale structure so evident in this case. Finally, we have shown that the two regions of PMS found during this period coincided with the above intervals of significant correlation between the two GCR time series. Further analyses utilizing high time resolution observations of GCR variations should shed more light on the importance of such structure to these and similar events.

Tony Bird, and Stephane Paltani, for useful discussions and help using the INTEGRAL data.

References

Barnden, L. R. (1973a), Forbush decreases 1966–1972: Their solar and interplanetary associations and their anisotropies, *Proc. 13th Int. Cosmic Ray Conf.*, *2*, 1271–1276.

Barnden, L. R. (1973b), The large-scale magnetic field configuration associated with forbush decreases, *Proc. 13th Int. Cosmic Ray Conf.*, *2*, 1277–1282.

Biermann, L. (1951), Kometenschweife und solare Korpuskularstrahlung, *Z. Astrophys.*, *29*, 274–286.

Biermann, L. (1957), Solar corpuscular radiation and the interplanetary gas, *Observatory*, *77*, 109–110.

Blake, J. B., et al. (1995), Ceppad, *Space Sci. Rev.*, *71*, 531–562, doi:10.1007/BF00751340.

Cane, H. V. (2000), Coronal mass ejections and forbush decreases, *Space Sci. Rev.*, *93*, 55–77, doi:10.1023/A:1026532125747.

Coleman, P. J., Jr., C. P. Sonett, D. L. Judge, and E. J. Smith (1960), Some preliminary results of the Pioneer V Magnetometer Experiment, *J. Geophys. Res.*, *65*, 1856–1857.

Contos, A. R. (1997), Complete description and characterization of the High Sensitivity Telescope (HIST) onboard the Polar satellite, Ph.D. thesis, Boston Univ., Boston, Mass.

de Koning, C. A. (2003), Probing the turbulent solar wind magnetic field with cosmic rays, Ph.D. thesis, Univ. of Del., Newark.

de Koning, C. A., and J. W. Bieber (2004), Probing heliospheric turbulence with cosmic rays: Theory, *Astrophys. J.*, *606*, 1200–1209, doi:10.1086/383177.

Dhanju, M. S., and V. A. Sarabhai (1967), Short-period variations of cosmic-ray intensity, *Phys. Rev. Lett.*, *19*, 252–254, doi:10.1103/PhysRevLett.19.252.

Fan, C. Y., P. Meyer, and J. A. Simpson (1960), Rapid reduction of cosmic-radiation intensity measured in interplanetary space, *Phys. Rev. Lett.*, *5*, 269–271, doi:10.1103/PhysRevLett.5.269.

Forbush, S. E. (1937), On the effects in cosmic-ray intensity observed during the recent magnetic storm, *Phys. Rev.*, *51*, 1108–1109, doi:10.1103/PhysRev.51.1108.3.

Forbush, S. E. (1954), World-wide cosmic-ray variations, 1937–1952, *J. Geophys. Res.*, *59*, 525–542.

Grigoryev, A. V., S. A. Starodubtsev, V. G. Grigoryev, I. G. Usoskin, and K. Mursula (2008), Fluctuations of cosmic rays and IMF in the vicinity of interplanetary shocks, *Adv. Space Res.*, *41*, 955–961, doi:10.1016/j.asr.2007.04.044.

Heber, B., J. Gieseler, P. Dunzlaff, R. Gómez-Herrero, A. Klassen, R. Müller-Mellin, R. A. Mewaldt, M. S. Potgieter, and S. E. S. Ferreira (2008), Latitudinal gradients of galactic cosmic rays during the 2007 solar minimum, *Astrophys. J.*, *689*, 1443–1447, doi:10.1086/592596.

Intriligator, D. S., J. R. Jokipii, T. S. Horbury, J. M. Intriligator, R. J. Forsyth, H. Kunow, G. Wibberenz, and J. T. Gosling (2001), Processes associated with particle transport in corotating interaction regions and near stream interfaces, *J. Geophys. Res.*, *106*, 10,625–10,634, doi:10.1029/2000JA000070.

Intriligator, D. S., A. Rees, and T. S. Horbury (2008), First analyses of planar magnetic structures associated with the Halloween 2003 events from the Earth to Voyager 1 at 93 AU, *J. Geophys. Res.*, *113*, A05102, doi:10.1029/2007JA012699.

Jean, P., et al. (2003), SPI instrumental background characteristics, *Astron. Astrophys.*, *411*, L107–L112, doi:10.1051/0004-6361:20031156.

Jokipii, J. R. (1969), Stochastic variations of cosmic rays in the solar system, *Astrophys. J.*, *156*, 1107–1116.

Jokipii, J. R., and J. Kóta (2000), Galactic and anomalous cosmic rays in the heliosphere, *Astrophys. Space Sci.*, *274*, 77–96.

Jokipii, J. R., and B. Thomas (1981), Effects of drift on the transport of cosmic rays. IV—Modulation by a wavy interplanetary current sheet, *Astrophys. J.*, *243*, 1115–1122, doi:10.1086/158675.

Jones, G. H., A. Rees, A. Balogh, and R. J. Forsyth (2002), The draping of heliospheric magnetic fields upstream of coronal mass ejecta, *Geophys. Res. Lett.*, *29*(11), 1520, doi:10.1029/2001GL014110.

Kóta, J. (1979), Drift—The essential process in losing energy, *Proc. 16th Int. Cosmic Ray Conf.*, *3*, 13–18.

Kuwabara, T., et al. (2004), Geometry of an interplanetary CME on October 29, 2003 deduced from cosmic rays, *Geophys. Res. Lett.*, *31*, L19803, doi:10.1029/2004GL020803.

McDonald, F. B. (2000), Integration of neutron monitor data with spacecraft observations: A historical perspective, *Space Sci. Rev.*, *93*, 263–284, doi:10.1023/A:1026552730290.

Morrison, P. (1956), Solar origin of cosmic-ray time variations, *Phys. Rev.*, *101*, 1397–1404, doi:10.1103/PhysRev.101.1397.

Munakata, K., et al. (2003), CME geometry deduced from cosmic ray anisotropy, *Proc. 28th Int. Cosmic Ray Conf.*, *6*, 3561–3564.

Nagashima, K., S. Sakakibara, K. Fujimoto, R. Tatsuoka, and I. Morishita (1990), Localized pits and peaks in Forbush decrease, associated with stratified structure of disturbed and undisturbed magnetic fields, *Nuovo Cimento C*, *13*, 551–587.

Nakagawa, T., A. Nishida, and T. Saito (1989), Planar magnetic structures in the solar wind, *J. Geophys. Res.*, *94*, 11,761–11,775.

Neugebauer, M., D. R. Clay, and J. T. Gosling (1993), The origins of planar magnetic structures in the solar wind, *J. Geophys. Res.*, *98*, 9383–9389.

Owens, A. J., and J. R. Jokipii (1972), Cosmic-ray scintillations: 1. Inside the magnetosphere, *J. Geophys. Res.*, *77*, 6639–6655.

Owens, A. J., and J. R. Jokipii (1973), Interplanetary scintillations of cosmic rays, *Astrophys. J.*, *181*, L147–L150.

Parker, E. N. (1958a), Dynamical instability in an anisotropic ionized gas of low density, *Phys. Rev.*, *109*, 1874–1876, doi:10.1103/PhysRev.109.1874.

Parker, E. N. (1958b), Cosmic-ray modulation by solar wind, *Phys. Rev.*, *110*, 1445–1449, doi:10.1103/PhysRev.110.1445.

Parker, E. N. (2001), A history of early work on the heliospheric magnetic field, *J. Geophys. Res.*, *106*, 15,797–15,802, doi:10.1029/2000JA000100.

Shea, M. A., and D. F. Smart (1990), A summary of major solar proton events, *Sol. Phys.*, *127*, 297–320.

Simpson, J. A. (1954), Cosmic-radiation intensity-time variations and their origin. III. The origin of 27-day variations, *Phys. Rev.*, *94*, 426–440, doi:10.1103/PhysRev.94.426.

Smart, D. F., M. A. Shea, and E. O. Flückiger (2000), Magnetospheric models and trajectory computations, *Space Sci. Rev.*, *93*, 305–333, doi:10.1023/A:1026556831199.

Sonnerup, B. U. O., and M. Scheible (2000), ISSI book on analysis methods for multi-spacecraft data, in *Analysis Methods for Multi-Spacecraft Data*, edited by G. Paschmann and S. J. Schwartz, *ESA Spec. Publ.*, *449*, 185–220.

Starodubtsev, S. A., and I. G. Usoskin (2003), Long-term modulation of the galactic cosmic-ray fluctuation spectrum, *Astron. Lett.*, *29*, 594–598, doi:10.1134/1.1607497.

Starodubtsev, S. A., et al. (2005), Long-term modulation of the cosmic ray fluctuation spectrum: Spacecraft measurements, *Proc. 29th Int. Cosmic Ray Conf.*, *2*, 247–250.

Starodubtsev, S. A., I. G. Usoskin, A. V. Grigoryev, and K. Mursula (2006), Long-term modulation of the cosmic ray fluctuation spectrum, *Ann. Geophys.*, *24*, 779–783.

Storini, M. (2000), Transient phenomena in the heliosphere and terrestrial effects, *Proc. 26th Int. Cosmic Ray Conf.*, *516*, 120–138.

Teegarden, B. J., P. Jean, G. Weidenspointner, J. Knödlseder, G. K. Skinner, P. von Ballmoos, C. Shrader, S. Sturner, and K. Watanabe (2004), Characterization and prediction of the SPI background, in *Proceedings of 5th INTEGRAL Workshop on the INTEGRAL Universe*, edited by V. Schoenfelder, G. Lichti, and C. Winkler, *ESA Spec. Publ.*, *552*, 819–822.

Vedrenne, G., et al. (2003), SPI: The spectrometer aboard INTEGRAL, *Astron. Astrophys.*, *411*, L63–L70, doi:10.1051/0004-6361:20031482.

Wimmer-Schweingruber, R. F., et al. (2006), Understanding interplanetary coronal mass ejection signatures, *Space Sci. Rev.*, *123*, 177–216, doi:10.1007/s11214-006-9017-x.

————————

J. B. Blake and T. Mulligan, The Aerospace Corporation, 2350 El Segundo Boulevard, El Segundo, CA 90245, USA.

M. Galametz, Laboratoire AIM, Université Paris Diderot, DAPNIA, Service d'Astrophysique, CEA, DSM, CNRS, F-91191 Gif-sur-Yvette, France.

A. P. Jordan and H. E. Spence, Department of Astronomy, Boston University, 725 Commonwealth Avenue, Room 514, Boston, MA 02215, USA. (apj2@bu.edu)

D. N. A. Shaul, High Energy Physics Group, Department of Physics, Imperial College London, London, UK.